Early and Selective Impairments in Axonal Transport Kinetics of Synaptic Cargoes Induced by Soluble Amyloid β-Protein Oligomers

Yong Tang[1,2], **David A. Scott**[1,2], **Utpal Das**[1,2], **Steven D. Edland**[2], **Kryslaine Radomski**[1,2,3], **Edward H. Koo**[2], and **Subhojit Roy**[1,2,*]

[1]Department of Pathology, University of California, San Diego, 9500 Gilman Drive, La Jolla, CA 92093, USA

[2]Department of Neurosciences, University of California, San Diego, 9500 Gilman Drive, La Jolla, CA 92093, USA

Abstract

The downstream targets of amyloid β (Aβ)-oligomers remain elusive. One hypothesis is that Aβ-oligomers interrupt axonal transport. Although previous studies have demonstrated Aβ-induced transport blockade, early effects of low-n soluble Aβ-oligomers on axonal transport remain unclear. Furthermore, the cargo selectivity for such deficits (if any) or the specific effects of Aβ on the motility kinetics of transported cargoes are also unknown. Toward this, we visualized axonal transport of vesicles in cultured hippocampal neurons treated with picomolar (p_M) levels of cell-derived soluble Aβ-oligomers. We examined select cargoes thought to move as distinct organelles and established imaging parameters that allow organelle tracking with consistency and high fidelity – analyzing all data in a blinded fashion. Aβ-oligomers induced early and selective diminutions in velocities of synaptic cargoes but had no effect on mitochondrial motility, contrary to previous reports. These changes were *N*-methyl D-aspartate receptor/glycogen synthase kinase-3β dependent and reversible upon washout of the oligomers. Cluster-mode analyses reveal selective attenuations in faster-moving synaptic vesicles, suggesting possible decreases in cargo/motor associations, and biochemical experiments implicate tau phosphorylation in the process. Collectively, the data provide a biological basis for Aβ-induced axonal transport deficits.

Keywords

amyloid β-oligomers; axonal transport; cargo-motor regulation; molecular motors; synaptic loss; transport packets

Available evidence strongly implicate amyloid-β (Aβ)-oligomers in the pathogenesis of Alzheimer's disease (AD) – key features of which include learning/memory deficits and synaptic losses (1). Although the known effects of Aβ-oligomers on synaptic plasticity provide a basis for the memory deficits, these alterations cannot readily explain the widespread loss of synapses seen in AD brains upon autopsy. One hypothesis is that Aβ-induced inhibition of axonal transport can diminish the delivery of cargoes to synapses, eventually leading to synaptic losses (2). This notion is also supported by the presence of

*Corresponding author: Subhojit Roy, MD, PhD, s1roy@ucsd.edu.
[3]Current address: Department of Anatomy, Physiology and Genetics, Uniformed Services University of the Health Sciences, 4301 Jones Bridge Road, Bethesda, MD 20814, USA

focal neuritic accumulations – 'dystrophic neurites' representing axonal transport impairments – that are commonly seen around dense-core Aβ-plaques.

Several studies have evaluated axonal transport in the presence of Aβ. Such studies have typically used high (micromolar) levels of synthetic Aβ, applied to cultured neurons for prolonged periods, resulting in dramatic and irreversible interruptions of transport frequencies (or flux) – often a near-complete stoppage of transport – true for a variety of cargoes including generic vesicles, mitochondria and markers of dense-core vesicles (3–6). Such global and irreversible impairments in trafficking evoke the possibility that Aβ may induce non-specific damage to axonal transport in these experimental settings; especially pertinent given its well-known cytotoxic nature. Another recent study perfused Aβ-oligomers in isolated squid axons that resulted in alterations of vesicular transport velocities, and also biochemically demonstrated a diminution of cargo-motor associations in this setting (7). However, the role of intracellular Aβ in AD is controversial (8), and the pathologic events underlying transport deficits in a mammalian system are still not fully resolved.

Toward this, we designed unbiased experiments to evaluate early effects of picomolar cell-derived extracellular Aβ-oligomers on the axonal transport kinetics of various cargoes. We optimized imaging parameters in cultured hippocampal neurons to quantify transport dynamics with high fidelity and analyzed the data with cluster-mode modeling. Soluble Aβ-oligomers induced diminutions in velocities of synaptic cargoes, but with no effects on mitochondrial motility, unlike previous reports (4–6). Interestingly, our modeling data suggest Aβ-provoked diminutions in the attachment/activation of motors to mobile vesicles, as suggested by Pigino et al. (7), and also implicate tau in this process.

Results

Experimental design and high-resolution imaging of axonal transport

The experimental strategy is outlined in Figure 1A. Days *in vitro* 14 (DIV 14) cultured mouse hippocampal neurons were treated with picomolar levels of cell-derived Aβ-oligomers (see below), and axonal transport of various transfected cargoes was imaged at a high temporal resolution (upto 5 frames/second) in primary axons. The cell-derived Aβ-oligomers used here have been well characterized and has been used in many previous studies (9, 10). Briefly, these oligomers are naturally secreted in the conditioned medium of Chinese hamster ovary (CHO) cells stably transfected with the V717F [amyloid precursor protein (APP)] mutation (also called the 7PA2 cell line). The 7PA2 cell line secretes high levels of soluble monomeric/small oligomeric-Aβ, with no insoluble aggregates (11), and the oligomeric species are thought to be similar to those found in human AD brains (12). For our experiments, the conditioned media (CM) is harvested, and appropriate concentrations are directly applied to cultured neurons (see *Materials and Methods* and below). For controls, CM of untransfected CHO cells (called CHO here) were used in all experiments. The terms '7PA2' and 'CHO' are used throughout the manuscript (including figures) to indicate Aβ-treated and Aβ-free experimental groups.

First, we evaluated effects of cell-derived Aβ-oligomers on spines. Neurons were incubated with oligomeric-Aβ (200 p$_M$ Aβ-42, measured by enzyme-linked immunosorbent assay (ELISA) – see *Materials and Methods*), and spines were quantified using established procedures (13). As shown in Figure 1B, treatment of neurons with 7PA2-media for 2 h reduced overall spine densities that were rescued by an *N*-methyl ᴅ-aspartate receptor (NMDA-R) inhibitor as reported previously (9). As 2 h is one of the earliest time-points at which spine changes occur in this system (9), we chose to first evaluate axonal transport at 2 h as well. We also optimized our transport imaging, adopting a strategy involving short-term imaging with high frame rates that allowed us to image fast-moving cargoes with optimal

fidelity in these mature cultures (see *Materials and Methods* for details and Movies S1–S3). Only primary axons, unequivocally identified as emerging from the soma, were imaged. Although particles in a given axon expectedly moved at a range of velocities (for a given cargo), the data range using these experimental parameters were quite consistent across different axons within a coverslip as well as axons from different culture sets (see raw velocity data distributions in Figure 1C), providing confidence in the validity of our approach.

Effects of soluble Aβ-oligomers on axonal transport

We evaluated axonal transport of three selected cargoes – synaptophysin, bassoon and mitochondria – as previous studies suggest that they represent distinct transport organelles. Specifically, while several synaptic transmembrane proteins are cotransported as pleomorphic tubulovesicular 'synaptic vesicle precursors' (SVP) or 'transport packets'; components of dense-core vesicles (piccolo, bassoon, RIM, etc.) are conveyed as distinct carriers called piccolo transport vesicles or PTV (14) – also reviewed in (15). Thus, we reasoned that synaptophysin and bassoon may serve as fiduciary markers for SVP/PTV respectively, allowing us to sample a range of synaptic cargoes. We also evaluated mitochondrial transport as previous studies have reported inhibition of mitochondrial transport upon treatment with synthetic Aβ (4–6). Average velocities of both synaptic cargoes were selectively diminished upon Aβ-treatment, with no detectable changes in mitochondrial transport (Figure 2A–C; also see composite transport data in Table 1).

Importantly, transport frequencies of all cargoes were unchanged upon Aβ-treatment (Table 2), indicating that the low levels of cell-derived Aβ-oligomers did not result in a generic blockade of transport frequencies. The Aβ-induced transport inhibition of bassoon/dense core vesicle (DCV) was bidirectional, whereas only anterograde synaptophysin/SVP velocities were diminished. Although the retrograde inhibition of DCV is interesting, in this study, we focused our attention on effects of Aβ upon anterograde transport kinetics. Anterograde run lengths of synaptophysin cargoes were also inhibited by Aβ, with diminishing trends in run lengths of bassoon cargoes as well (Figure 2C, bottom). Transport abnormalities of synaptophysin cargoes was abrogated upon incubation with Aβ-

immunodepleted 7PA2 media (see *Materials and Methods*), indicating that these deficits were specific for Aβ (data not shown).

Rescue/recovery of transport deficits by NMDA-R and GSK-3β inhibitors and oligomer washout

Aβ-mediated changes in synaptic plasticity are thought to be mediated via an NMDA-R- and glycogen synthase kinase-3β (GSK-3β)-dependent mechanism (16), and a recent study showed that transport deficits induced by synthetic Aβ-oligomers were partially rescued by NMDA-R/GSK-3β inhibitors (5). Accordingly, we next asked whether the transport deficits seen in our system were also mediated via this pathway. Neurons were coincubated with 7PA2-CM as well as the NMDA-R inhibitors MK801 (or DAP-5) for 2 h, and axonal transport was analyzed. Indeed, these treatments rescued the synaptophysin transport deficits. All impairments in synaptophysin and bassoon were also rescued by the selective GSK-3β inhibitor GSK-VIII (Fig. 3A,B).

To our knowledge, no transport study has demonstrated reversibility of Aβ-induced transport deficits upon clearance of Aβ; rather, when reported, synthetic Aβ-oligomers induce irreversible transport blockade (3). As axonal transport is exquisitely sensitive to changes in neuronal physiology (our empiric observations), this issue is important to preclude potential non-specific and irreversible toxic effects of Aβ-oligomers that may result in a generic transport blockade. Accordingly, we incubated neurons with 7PA2-media for 2 h, transferred them into a medium containing fresh (Aβ-free) media for another 22 h and then visualized synaptophysin transport – appropriate controls were run in parallel (see experimental design in Figure 4A). Washout of the oligomers rescued all Aβ-induced transport deficits (Figure 4B, top). Similar experiments were also performed with oligomeric-Aβ (200 p_M) incubations for 24 h (Figure 4B, bottom).

Specific attenuation of faster velocity peaks by soluble Aβ-oligomers

What are the specific effects of Aβ-oligomers on cargo motility? Although previous studies have reported global Aβ-induced impairments in transport frequencies (3–6), the specific effects on axonal transport kinetics have not been examined. Our optimized imaging parameters captured transported cargo kinetics with high fidelity and allowed us to address this issue in our studies. We first statistically determined the modes (peaks) of average velocity distributions in control (CHO) and Aβ-treated (7PA2) axons using established cluster-mode analysis algorithms (17, 18). Essentially, these algorithms automatically assign single or multiple Gaussians to data distributions in an unbiased fashion, solely based on the clustering of raw data points (see *Materials and Methods* for details and Figure S1A).

Interestingly, the average anterograde velocity distribution of synaptophysin and bassoon was non-normal and best fitted by a two-Gaussian distribution with approximate peaks of $1\times$ and $2\times$ periodicity (Figures 5A and [S1A]). What do these multiple 'velocity peaks' represent? Previous studies on vesicle transport with nanometer resolution have also reported multiple spikes in average cargo velocities with approximately regular periodicity (19, 20). Such multiple peaks are also seen in a variety of other model systems (21, 22). Although the underlying reasons for such 'velocity peaks' is controversial (see below), some studies have attributed them to a quantitative gain or loss of active molecular motors on vesicular cargoes during transit within a viscous cytoplasmic environment (19).

Such a gain/loss of motor activity could arise either due to a change in the *number* of motors physically attached to cargoes or due to altered *activation* of associated motors with no changes in motor numbers (19–22). However, it is important to note that this interpretation

is not universally accepted, and some studies have failed to see multimodal velocity peaks despite rigorous quantitative analyses (23).

Intriguingly, however, incubation with Aβ-oligomers for 2/24 h led to a clear diminution of the second (faster) peaks (Figure 5A,B, top rows) of synaptophysin cargoes, resulting in significant Aβ-induced changes of waveform proportions between the CHO/7PA2 groups (p = 0.010) and p << 0.001 for 2/24 h, respectively (see *Materials and Methods* for statistical details). These diminutions were largely offset upon treatment with GSK3β inhibitors (Figure 5A,B, bottom rows), as well as upon incubation with the NMDA-R inhibitors MK801 and DAP-5 (Figure S1B). A similar diminution of faster velocity peaks – albeit somewhat lesser in magnitude – was also seen in anterograde bassoon transport (Figure 6A, top panels), that was also offset by incubation with the GSK-3β-inhibitor (Figure 6A, bottom panels); however, velocity peaks of mitochondrial transport were unimodal (Figure 6B). These data indicate that Aβ-oligomers induce a selective diminution of faster-moving synaptic vesicles. Following the arguments above, one interpretation of these data is that low-n soluble Aβ-oligomers may result in attenuated association/activation of vesicular cargoes to motors. To further explore this issue, we biochemically evaluated levels of kinesins associated with vesicles – incubating neurons with Aβ-oligomers and immunoblotting cell lysates with synaptophysin and kinesin antibodies. However, we could not detect significant reductions in the protein levels of kinesin heavy or light chains (data not shown). Notably, there were clear increases in phosphorylated tau levels upon incubation with Aβ-oligomers with no changes in total tau, as shown in Figure 7A,B.

Discussion

Although previous studies have shown that Aβ peptides can induce axonal transport deficits, the effects of extracellular, low-n Aβ-oligomers on mobile cargoes have not been explored. Moreover, all studies to date have demonstrated global deficits in all examined cargoes, and the cargo selectivity of such transport deficits (if any) or the specific effects of Aβ on cargo kinetics is unknown. In this study, we evaluated effects of low-n soluble Aβ-oligomers on axonal transport of rationally selected cargoes with high temporal resolution. Aβ-oligomers resulted in specific impairments in transport velocities and run lengths of synaptic cargoes, but with no changes in mitochondrial motility, unlike previous reports. These impairments were mediated via an NMDA-R/GSK-3β-dependent pathway and were also reversible upon Aβ removal. Cluster-mode modeling of velocity data and biochemical studies indicate that Aβ-oligomers lead to selective impairments of faster velocity peaks, but levels of motor proteins remain unchanged, suggesting that Aβ-oligomers may ultimately lead to diminished activation of molecular motors associated with vesicles.

Use of low-n soluble Aβ-oligomers to evaluate axonal transport

Previous studies evaluating axonal transport in the presence of Aβ have typically incubated cultured neurons with micromolar amounts of synthetic Aβ, resulting in dramatic reductions of transport frequencies (or flux) of all moving cargoes – typically an almost complete transport blockade (3–6). Although these studies indicate that Aβ impairs transport, a reduced overall flux could also result from Aβ-induced non-specific toxicity (e.g. defects in vesicle biogenesis or endoplasmic reticulum to Golgi transport induced by Aβ) that would also impair axonal transport. Moreover, when reported, transport deficits induced by synthetic Aβ are irreversible (3), again invoking issues related to generic Aβ-related toxicity. It should be noted that the Aβ-42 levels in our studies is 200 p_M, the minimal amount that results in synaptic toxicity in our system [see Figure 1 and also Ref. (9)]. However, synthetic Aβ levels used in previous transport studies are in the micromolar range (3–6). These differences are several orders of magnitude apart, and it seems reasonable to

imagine that the high levels of Aβ used in prior transport studies would lead to some amount of non-specific toxicity that would secondarily affect axonal transport.

Toward this, we designed experiments using low levels of cell-derived Aβ-oligomers and visualized transport using optimized imaging parameters that allowed us to clearly visualize and quantify mobile particles (Movies S1–S3). These oligomers have been used by many previous studies and largely consist of low-n dimers and trimers (10, 11). Importantly, these experimental conditions did not result in significant blockade of overall transport frequencies (Table 2) but instead led to a diminution in the velocities of selected cargoes. Also, these changes were reversible upon Aβ removal, indicating a discrete and specific effect of Aβ on the transport machinery moving vesicular cargoes.

Cargo selectivity of Aβ-induced transport deficits

We found that low-n Aβ-oligomers do not result in global transport deficits as previously reported. Specifically, while transport of SVP/PTV synaptic cargoes was affected, transport parameters of mitochondria remain unchanged (no diminution of mitochondrial transport was seen even after 24 h of 7PA2 incubation – data not shown). Notably, mitochondrial transport dynamics are somewhat different from that of other cargoes. Kinesin heavy chains are reported to directly associate with mitochondria (24), and run lengths of mitochondria are also several fold higher than synaptic cargoes (Figure 2C), suggesting that the motors may be continuously engaged to mitochondria for very long periods. As our modeling data (Figures 5 and 6 and see *Discussion* below) suggest that Aβ-oligomers may lead to decreased cargo-motor engagement, one possible explanation for a lack of inhibition of mitochondrial transport is that such Aβ-induced transport defects are most pronounced for synaptic (and possibly other) cargoes that have a greater rate of cargo attachment/ detachment; but more continuously engaged cargoes such as mitochondria are relatively spared.

These data raise the question whether the Aβ-induced inhibition of mitochondrial motility as reported by other studies are a result of generic Aβ toxicity. Finally, we note that although previous studies have shown that similar treatments with picomolar Aβ-oligomers (7PA2 media) lead to electrophysiologic changes (9), it is difficult to establish a cause and effect relationship of the transport interruptions seen in our studies with known Aβ-induced functional deficits.

Aβ-oligomers may diminish activation of multiple motors associated with mobile cargoes

The temporal resolution of our transport studies allowed us to dissect effects of Aβ-oligomers on cargo kinetics. Specifically, histograms of velocity distributions of synaptophysin could be best fitted by two-Gaussian peaks with approximate 1× and 2× periodicity (Figures S1A and 5, 6). Similar multimodal peaks have also been reported in other studies that have examined transport kinetics with high resolution (19–21), and one interpretation is that different vesicle populations are transported by differing copy numbers of a given motor protein, moving in a viscous environment (19). Alternatively, in a cellular environment, the number of attached motors to vesicles may remain the same, but some motors may be selectively activated. Indeed, it is generally accepted that multiple (but a small number) of motors are responsible for moving individual cargoes (25, 26). However, as noted above, such velocity peaks are not universally seen, and the above interpretation of velocity peaks has been questioned on these grounds (23). Although our studies are indirect and do not address this controversy in any way, perhaps the presence/absence of peaks may depend on the nature of the cargo examined and/or the assortment of associated/ activated motors.

Nevertheless, it is interesting that Aβ-oligomers resulted in a selective diminution (flattening) of the higher velocity peak of synaptophysin (Figure 5) that was abrogated either by treatment with a GSK-3β inhibitor or by NMDA-R blockade (Figures 5 and [S1B]). If indeed these faster velocity peaks represent incremental association/activation of motors to vesicles as suggested by the above studies, one interpretation is that Aβ-oligomers either lead to a physical diminution in the attachment of motors to cargoes or lead to a reduced activation of motors that are already attached to vesicles. Toward the former, GSK-3β activation can phosphorylate (and detach) kinesin light chains from vesicles, resulting in slowing/stalling of transported cargoes (27) and such a mechanism could potentially explain our transport deficits. Alternatively, it is also possible that the association/activation of motors is influenced by an (Aβ-mediated) increase in tau levels (28, 29). We could not detect any significant change in the protein levels of kinesin heavy and light chains (normalized to synaptophysin levels) in 7PA2-treated neurons compared to controls; however, there were clear increases in relative levels of tau phosphorylation (but not total tau) in our system (Figure 7). Recent studies in cultured neurons also implicate Aβ-induced increases in tau phosphorylation as the harbinger of Aβ-related neuritic pathology (30, 31), and our data support this notion. Thus, in aggregate, these data suggest that Aβ-induced changes in transport may be mediated via selective deactivation of motors already associated with cargoes; however, more focused work is needed to clarify these issues.

The purpose of this study was to evaluate the early effects of picomolar levels of low-n soluble Aβ-oligomers on mobile cargoes, using a rational experimental approach. Although the precise consequence of these transport disruptions on the pathogenesis of AD *in vivo* remains to be established, we note that the relatively modest transport deficit seen in our experiments (about 20% diminution) is perhaps a more reasonable pathologic substrate of a slowly progressive disease like AD, as opposed to the dramatic and abrupt transport interruptions seen when using Aβ levels that are several orders of magnitude higher than the picomolar to low nanomolar levels reported in the brains of AD patients (32) or AD mouse models (33).

Materials and Methods

Plasmids and reagents

DsRed-mitochondria was obtained from Clontech; synaptophysin: monomeric red fluorescent protein (mRFP) and bassoon:green fluorescent protein (GFP) were gifts from Leon Laganado (MRC) and Craig Garner (Stanford). The specific GSK-3β-inhibitor VIII (AR-A014418) was from Calbiochem. Specificity has been shown using a panel of 28 different kinases including Cdk2 and Cdk5. MK-801 was from Sigma and D-AP5 was from Tocris Biosciences.

Hippocampal cultures, transfections

Primary hippocampal neurons were obtained from postnatal (P0–P1) CD-1 mice as described previously (34). Briefly, dissociated cells were plated at a density of 50,000 cells/cm^2 in poly-ᴅ-lysine coated (1.0 mg/mL) glass-bottom culture dishes (MatTek). Cultures were maintained in Neurobasal/B27 media (Invitrogen) supplemented with 0.5 mᴍ glutamine. For axonal transport experiments, DIV 12–14 cells were transfected (Lipofectamine) with the respective constructs as well as a soluble GFP or mRFP marker. This allowed clear visualization of the dendritic and axonal morphology and allowed us to selectively evaluate transport in primary axonal shafts only. Only neurons where the morphology of the primary axon was favorable, and could be unequivocally traced as emerging from the cell body, were used for transport imaging [also see Ref. (35) for generic details of transport imaging]. All imaging studies were performed 17–24 h posttransfection,

and low expressers were selected for all transport imaging. Animal studies were performed in accordance with University of California guidelines.

Preparation of cell-derived Aβ-oligomers

Aβ-oligomers were obtained from the CM of CHO cells expressing the V717F mutation in the APP, essentially as described before (11, 9), with the exception that a Hibernate-E-based 'live-imaging media' was used as the conditioning medium (36). Briefly, transfected/ untransfected CHO cells were grown to confluency, and the 'live-imaging medium' was conditioned by incubation with the CHO cells for 16 h.Media was then cleared of debris $(200 \times g$, 10 min at 4°C), flash-frozen in aliquots and stored at −80°C. This was diluted in the 'live-imaging medium' to a final concentration of 200 p$_M$ before application. The total Aβ concentration was established by ELISA using the monoclonal antibody Ab9 as capture (37) and biotin-coupled 4G8 (Signet Labs) as reporter.

Microscopy and live imaging

All time-lapse movies and dendritic spine images were acquired using an Olympus IX81 inverted epifluorescence microscope equipped with a Z-controller (IX81, Olympus), a motorized X-Y stage controller (Prior Scientific) and a fast electronic shutter (SmartShutter). Images were acquired using an ultra-stable light source (Exfo exacte) and high-performance CCD cameras (Coolsnap HQ^2, Photometrics). For live imaging, neurons were transferred to a Hibernate-E-based 'live-imaging' media (with the appropriate conditioned medium from CHO or 7PA2 cells) and imaged at 35–37°C, maintained with an air-curtain incubator (Nevtek) mounted on the microscope. All images were acquired using METMAMORPH software (Molecular Devices) and processed using either METAMORPH or IMAGE J. Movies of synaptophysin and bassoon were acquired at 5 frames/second and 200-millisecond exposure (with no interval between frames) using the 'stream acquisition' mode in METAMORPH. Each axon was imaged for a total of 15 seconds, with no neutral-density filters in the light path. Such high time-compression/low-duration imaging parameters enabled clear visualization of all moving particles and vastly enhanced the quality of the data set, allowing us to analyze these particles from kymographs. Mitochondrial images were acquired at 1 frame/3 seconds and ≈200–400-millisecond exposure. As mitochondrial velocities are much slower and the transport is infrequent, these parameters are expected to reveal all mitochondrial dynamics (38). For dendritic spine imaging, DIV 17–21 neurons were transfected with soluble GFP and treated with CHO/7PA2 for 2 h. GFP-positive spines were analyzed using Z-series imaging followed by deconvolution (Huygens) as described previously (34).

Image analysis

Transport was analyzed from kymographs by an observer blinded to the experimental conditions. Kymographs were generated in METAMORPH, and segmental tracks were overlaid on the kymographs using a line tool. The resultant velocity data (distance/time) was obtained for each track. The high temporal resolution and short imaging duration generated high-fidelity kymographs that had limited numbers of mobile particles, making such analyses feasible. When needed, kymographs were also stretched along the y-axes using 'stretch and mirror' to facilitate track visualization; all tracks were saved as '.rgn' files in METAMORPH. All uninterrupted tracks that displayed a minimum velocity of 0.32 μm/second and minimum run length of 0.72 μm were analyzed. These criteria were applied throughout the study. Particles that remained immobile for the duration of the imaging period were considered as stationary. Frequencies of particle movements were determined by dividing the number of individual particles moving in a given direction by the total number of particles in the kymograph. Routine statistical comparisons were performed using PRISM software (Graphpad)

using the Student's *t*-test (for comparing two groups) or one-way ANOVA (for comparing multiple groups). Spines were analyzed by observers blinded to the experimental conditions, using previously established morphologic criteria (13).

Cluster-mode analyses

Predicted Gaussian modes were fitted using the MCLUST package in the R statistical computing environment (17, 18) with parameter estimation of mean velocity peaks, and standard deviations by maximum likelihood [(17, 18) and see Figure S1A]. The raw velocity distributions of synaptophysin and bassoon (as determined by the software) were non-normal and were best fitted by a two-Gaussian distribution. For comparing the CHO and 7PA2 data sets, relative proportions of the two peaks classified as slow or fast (classified as the first or second velocity modes) were statistically evaluated using a one-way Chi-square test. A p value of <0.05 indicated dissimilar peak proportions.

Biochemical assays

Cultured neurons were lysed in buffer containing 50 m$_M$ Tris–Cl, pH 7.6, 150 m$_M$ NaCl, 2 m$_M$ EDTA, 1% n-dodecyl-β-$_D$-maltoside and protease inhibitors (Sigma). Twenty micrograms of proteins from the postnuclear supernatant fraction was used for SDS–PAGE and western blotting using routine protocols. Immunoprecipitation (IP)/immunodepletion of Aβ from 7PA2 medium was done, following the protocol described by Shankar et al. (10). Briefly, 2 mL of 7PA2 and CHO-CM were precleared with 25 μL of protein A and 25 μL of protein G resin for 1 h at 4°C and collected the supernatant after centrifuging at $3500 \times g$ for 5 min. Precleared media were incubated with IP antibody 21F12 (3 μg/mL, gift from Elan Pharma) plus 15 μL protein A and 15 μL protein G resin for 3 h at 4°C with gentle shaking on a nutator. Supernatant was collected after centrifuging at $3500 \times g$ and used as immunodepleted media for cell culture experiments. Depletion of Aβ from the immunodepleted media (collected after the first IP) was confirmed by performing a second IP using the same protocol and probing with 6E10 antibody (Covance).

Acknowledgments

References

1. Haass C, Selkoe DJ. Soluble protein oligomers in neurodegeneration: lessons from the Alzheimer's amyloid beta-peptide. Nat Rev Mol Cell Biol. 2007; 8:101–112. [PubMed: 17245412]

2. Morfini GA, Burns M, Binder LI, Kanaan NM, LaPointe N, Bosco DA, Brown RH Jr, Brown H, Tiwari A, Hayward L, Edgar J, Nave KA, Garberrn J, Atagi Y, Song Y, et al. Axonal transport defects in neurodegenerative diseases. J Neurosci. 2009; 29:12776–12786. [PubMed: 19828789]

3. Hiruma H, Katakura T, Takahashi S, Ichikawa T, Kawakami T. Glutamate and amyloid beta-protein rapidly inhibit fast axonal transport in cultured rat hippocampal neurons by different mechanisms. J Neurosci. 2003; 23:8967–8977. [PubMed: 14523099]

4. Rui Y, Tiwari P, Xie Z, Zheng JQ. Acute impairment of mitochondrial trafficking by beta-amyloid peptides in hippocampal neurons. J Neurosci. 2006; 26:10480–10487. [PubMed: 17035532]

5. Decker H, Lo KY, Unger SM, Ferreira ST, Silverman MA. Amyloid-beta peptide oligomers disrupt axonal transport through an NMDA receptor-dependent mechanism that is mediated by glycogen synthase kinase 3beta in primary cultured hippocampal neurons. J Neurosci. 2010; 30:9166–9171. [PubMed: 20610750]

6. Vossel KA, Zhang K, Brodbeck J, Daub AC, Sharma P, Finkbeiner S, Cui B, Mucke L. Tau reduction prevents Abeta-induced defects in axonal transport. Science. 2010; 330:198. [PubMed: 20829454]

7. Pigino G, Morfini G, Atagi Y, Deshpande A, Yu C, Jungbauer L, LaDu M, Busciglio J, Brady S. Disruption of fast axonal transport is a pathogenic mechanism for intraneuronal amyloid beta. Proc Natl Acad Sci U S A. 2009; 106:5907–5912. [PubMed: 19321417]

8. Winton MJ, Lee EB, Sun E, Wong MM, Leight S, Zhang B, Trojanowski JQ, Lee VM. Intraneuronal APP, not free Abeta peptides in 3xTg-AD mice: implications for tau versus Abeta-mediated Alzheimer neurodegeneration. J Neurosci. 2011; 31:7691–7699. [PubMed: 21613482]

9. Calabrese B, Shaked GM, Tabarean IV, Braga J, Koo EH, Halpain S. Rapid, concurrent alterations in pre- and postsynaptic structure induced by naturally-secreted amyloid-beta protein. Mol Cell Neurosci. 2007; 35:183–193. [PubMed: 17368908]

10. Shankar GM, Welzel AT, McDonald JM, Selkoe DJ, Walsh DM. Isolation of low-n amyloid beta-protein oligomers from cultured cells CSF brain. Methods Mol Biol. 2011; 670:33–44. [PubMed: 20967581]

11. Walsh DM, Klyubin I, Fadeeva JV, Cullen WK, Anwyl R, Wolfe MS, Rowan MJ, Selkoe DJ. Naturally secreted oligomers of amyloid beta protein potently inhibit hippocampal long-term potentiation in vivo. Nature. 2002; 416:535–539. [PubMed: 11932745]

12. Shankar GM, Li S, Mehta TH, Garcia-Munoz A, Shepardson NE, Smith I, Brett FM, Farrell MA, Rowan MJ, Lemere CA, Regan CM, Walsh DM, Sabatini BL, Selkoe DJ. Amyloid-beta protein dimers isolated directly from Alzheimer's brains impair synaptic plasticity and memory. Nat Med. 2008; 14:837–842. [PubMed: 18568035]

13. Chapleau CA, Carlo ME, Larimore JL, Pozzo-Miller L. The actions of BDNF on dendritic spine density and morphology in organotypic slice cultures depend on the presence of serum in culture media. J Neurosci Methods. 2008; 169:182–190. [PubMed: 18242714]

14. Zhai RG, Vardinon-Friedman H, Cases-Langhoff C, Becker B, Gundelfinger ED, Ziv NE, Garner CC. Assembling the presynaptic active zone: a characterization of an active one precursor vesicle. Neuron. 2001; 29:131–143. [PubMed: 11182086]

15. Schlager MA, Hoogenraad CC. Basic mechanisms for recognition and transport of synaptic cargos. Mol Brain. 2009; 2:25. [PubMed: 19653898]

16. Li S, Hong S, Shepardson NE, Walsh DM, Shankar GM, Selkoe D. Soluble oligomers of amyloid Beta protein facilitate hippocampal long-term depression by disrupting neuronal glutamate uptake. Neuron. 2009; 62:788–801. [PubMed: 19555648]

17. Fraley C. MCLUST: software for model-based cluster analysis. J Classification. 1999; 16:297–306.

18. Fraley C, Raftery AE. Model-based clustering, discriminant analysis, and density estimation. J Am Stat Assoc. 2002; 97:611–631.

19. Kural C, Kim H, Syed S, Goshima G, Gelfand VI, Selvin PR. Kinesin and dynein move a peroxisome in vivo: a tug-of-war or coordinated movement? Science. 2005; 308:1469–1472. [PubMed: 15817813]

20. Levi V, Serpinskaya AS, Gratton E, Gelfand V. Organelle transport along microtubules in *Xenopus* melanophores: evidence for cooperation between multiple motors. Biophys J. 2006; 90:318–327. [PubMed: 16214870]

21. Zahn TR, Angleson JK, MacMorris MA, Domke E, Hutton JF, Schwartz C, Hutton JC. Dense core vesicle dynamics in *Caenorhabditis elegans* neurons and the role of kinesin UNC-104. Traffic. 2004; 5:544–559. [PubMed: 15180830]

22. Encalada SE, Szpankowski L, Xia CH, Goldstein LS. Stable kinesin and dynein assemblies drive the axonal transport of mammalian prion protein vesicles. Cell. 2011; 144:551–565. [PubMed: 21335237]

23. Shubeita GT, Tran SL, Xu J, Vershinin M, Cermelli S, Cotton SL, Welte MA, Gross SP. Consequences of motor copy number on the intracellular transport of kinesin-1-driven lipid droplets. Cell. 2008; 135:1098–1107. [PubMed: 19070579]

24. Cai Q, Sheng ZH. Mitochondrial transport and docking in axons. Exp Neurol. 2009; 218:257–267. [PubMed: 19341731]

25. Holzbaur EL, Goldman YE. Coordination of molecular motors: from in vitro assays to intracellular dynamics. Curr Opin Cell Biol. 2010; 22:4–13. [PubMed: 20102789]

26. Gross SP, Vershinin M, Shubeita GT. Cargo transport: two motors are sometimes better than one. Curr Biol. 2007; 17:R478–R486. [PubMed: 17580082]

27. Morfini G, Szebenyi G, Elluru R, Ratner N, Brady ST. Glycogen synthase kinase 3 phosphorylates kinesin light chains and negatively regulates kinesin-based motility. EMBO J. 2002; 21:281–293. [PubMed: 11823421]

28. Dixit R, Ross JL, Goldman YE, Holzbaur EL. Differential regulation of dynein and kinesin motor proteins by tau. Science. 2008; 319:1086–1089. [PubMed: 18202255]

29. Vershinin M, Carter BC, Razafsky DS, King SJ, Gross SP. Multiplemotor based transport and its regulation by Tau. Proc Natl Acad Sci U S A. 2007; 104:87–92. [PubMed: 17190808]

30. Jin M, Shepardson N, Yang T, Chen G, Walsh D, Selkoe DJ. Soluble amyloid beta-protein dimers isolated from Alzheimer cortex directly induce Tau hyperphosphorylation and neuritic degeneration. Proc Natl Acad Sci U S A. 2011; 108:5819–5824. [PubMed: 21421841]

31. Zempel H, Thies E, Mandelkow E, Mandelkow EM. Abeta oligomers cause localized Ca(2+) elevation, missorting of endogenous Tau into dendrites, Tau phosphorylation, and destruction of microtubules and spines. J Neurosci. 2010; 30:11938–11950. [PubMed: 20826658]

32. van Helmond Z, Miners JS, Kehoe PG, Love S. Higher soluble amyloid beta concentration in frontal cortex of young adults than in normal elderly or Alzheimer's disease. Brain Pathol. 2010; 20:787–793. [PubMed: 20175777]

33. Waters J. The concentration of soluble extracellular amyloidbeta protein in acute brain slices from CRND8 mice. PLoS One. 2010; 5:e15709. [PubMed: 21209950]

34. Scott DA, Tabarean I, Tang Y, Cartier A, Masliah E, Roy S. A pathologic cascade leading to synaptic dysfunction in alpha-synuclein-induced neurodegeneration. J Neurosci. 2010; 30:8083–8095. [PubMed: 20554859]

35. Roy S, Yang G, Tang Y, Scott DA. A simple photoactivation and image analysis module for visualizing and analyzing axonal transport with high temporal resolution. Nat Protoc. 2011; 7:62–68. [PubMed: 22179592]

36. Roy S, Winton MJ, Black MM, Trojanowski JQ, Lee VM. Rapid and intermittent cotransport of slow component-b proteins. J Neurosci. 2007; 27:3131–3138. [PubMed: 17376974]

37. Levites Y, Das P, Price RW, Rochette MJ, Kostura LA, McGowan EM, Murphy MP, Golde TE. Anti-Abeta42- and anti-Abeta40-specific mAbs attenuate amyloid deposition in an Alzheimer disease mouse model. J Clin Invest. 2006; 116:193–201. [PubMed: 16341263]

38. De Vos KJ, Sheetz MP. Visualization and quantification of mitochondrial dynamics in living animal cells. Methods Cell Biol. 2007; 80:627–682. [PubMed: 17445716]

A Experimental strategy
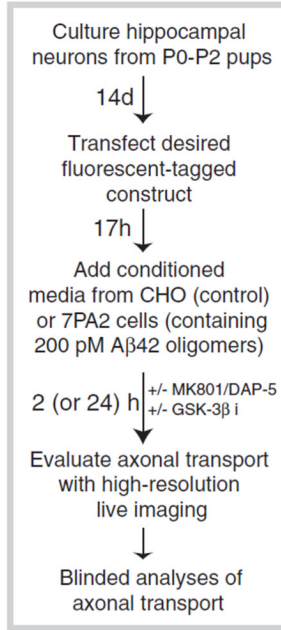
B Effects of cell-derived Aβ oligomers on dendritic spines
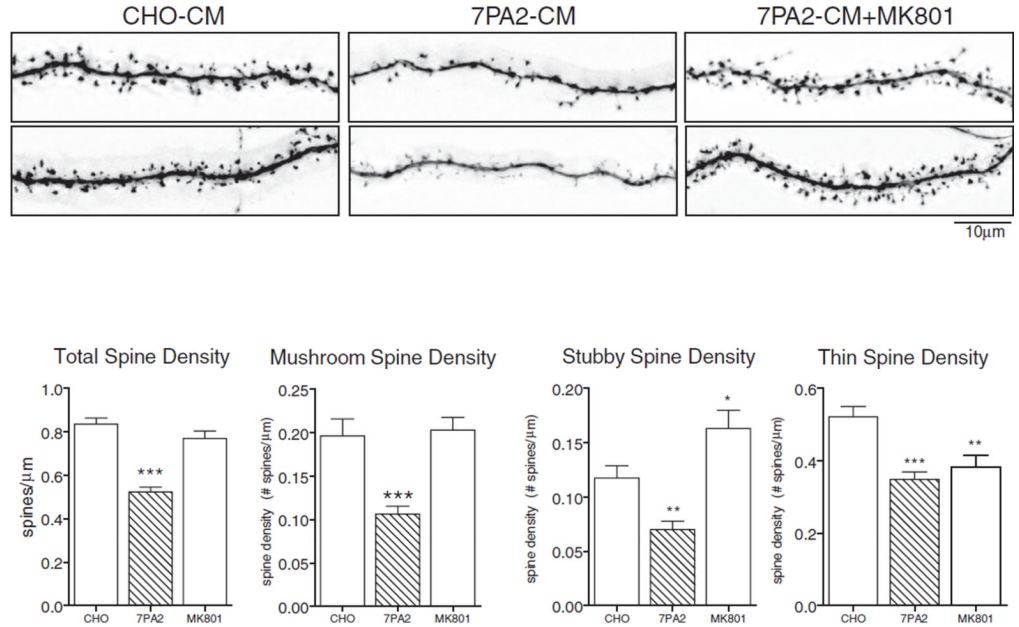
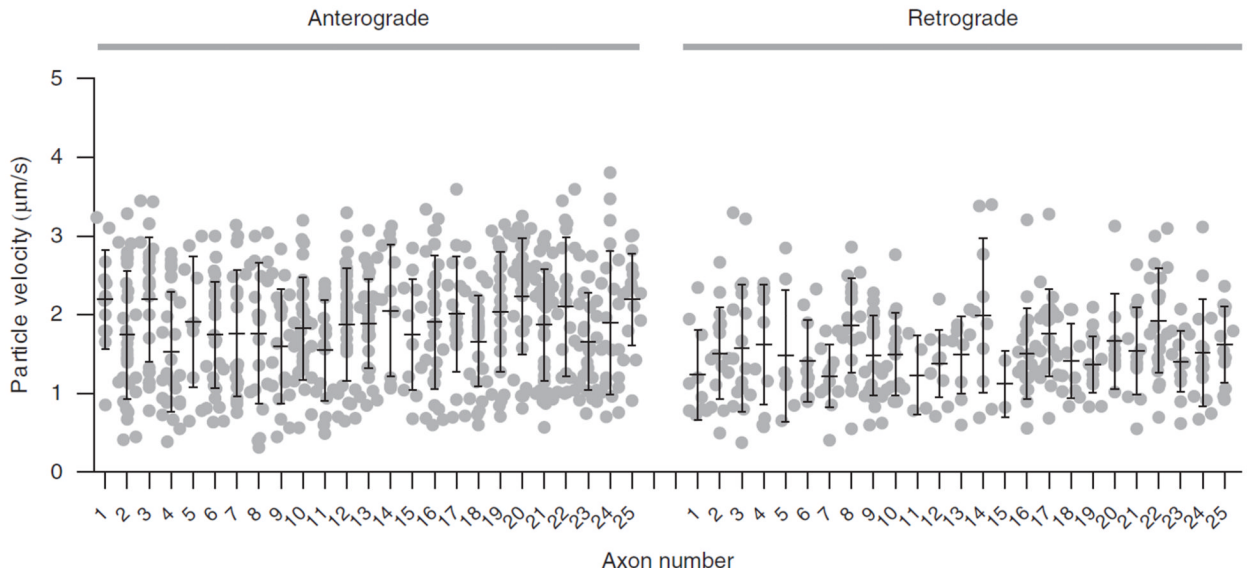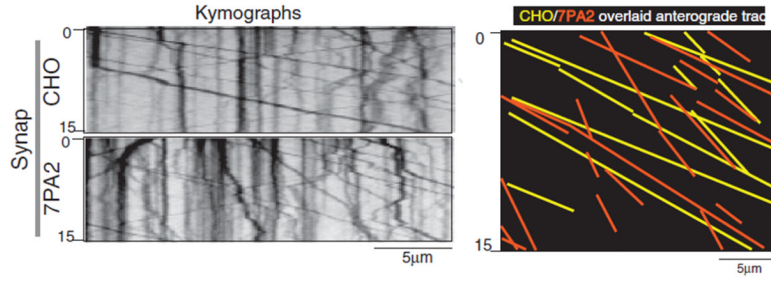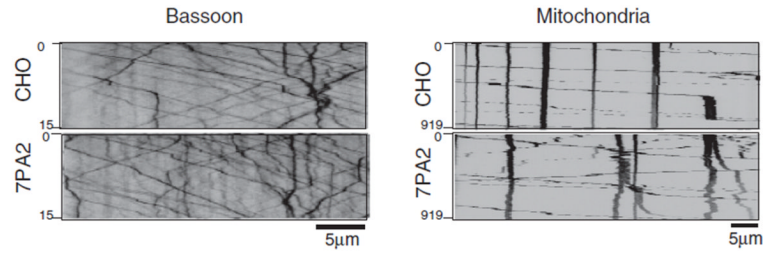**C Raw data-sets from high resolution transport imaging**

Figure 1. Overall experimental strategy and effects of cell-derived Aβ-oligomers on spines
A) Experimental strategy: Hippocampal neurons obtained from postnatal pups were cultured for 2 weeks, incubated with conditioned media (CM) containing cell-derived Aβ-oligomers (200 p$_M$ Aβ-42, called 7PA2) or control media (0 p$_M$ Aβ-42, called CHO) for 2 (or 24) h, axonal transport was imaged with high temporal resolution (upto 5 frames/second, see *Materials and Methods*), and the data were analyzed by an observer blinded to the experimental conditions. In some experiments, inhibitors of NMDA-R or GSK-3β were added as described in the text. B) To evaluate the effects of cell-derived Aβ-oligomers on spines, cultured neurons were incubated with 7PA2-CM (containing 200 p$_M$ Aβ-42) or CHO-CM (0 p$_M$ Aβ-42), and spine morphology was analyzed using established criteria (see

Materials and Methods). Note that Aβ-treatments led to a decrease in spine densities that was rescued by the NMDA-R inhibitor MK801. $n \approx$ 1100–1500 spines, *p < 0.05; **p < 0.01; ***p < 0.001; one-way ANOVA followed by Dunnet's post hoc test. C) Distribution of raw synaptophysin transport data points in 25 axons. Note that though there is an intrinsic variability in the instantaneous velocities of particles moving within a given axon (mean ± standard deviation for each axon is also shown), the overall range of velocities is similar across multiple axons (also note the overall differences in anterograde versus retrograde transport).

Figure 2. Selective inhibition of synaptic cargo transport by soluble Aβ-oligomers
A) Representative kymographs of synaptophysin: GFP transport from CHO (control) and 7PA2 (Aβ-treated) axons with overlaid anterograde tracks on right (raw tracks overlaid with yellow/red lines for CHO/7PA2, respectively); time in seconds: left of kymographs. Note the distinct slower velocity tracks in Aβ-treated axons. B) Representative kymographs from bassoon: GFP and DsRed-mito transport. C) Top: Mean average anterograde velocities of synaptophysin cargoes and bidirectional velocities of bassoon cargoes were lower in the Aβ-treated axons (7PA2 groups). Bottom: Similar trends were seen for the run lengths of various cargoes. Note that there are no detectable changes in mitochondrial transport (see Table 1 for numerical data). Transport frequencies were similar in all groups (see Table 2
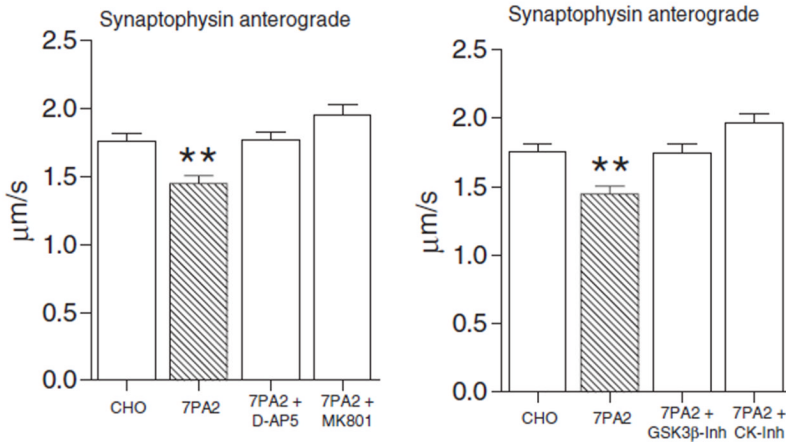
for numerical data). $n \approx 300 - 500$ moving particles analyzed for each cargo, from at least two separate sets of cultures. *p < 0.05; **p < 0.01; ***p < 0.001; unpaired t-test.
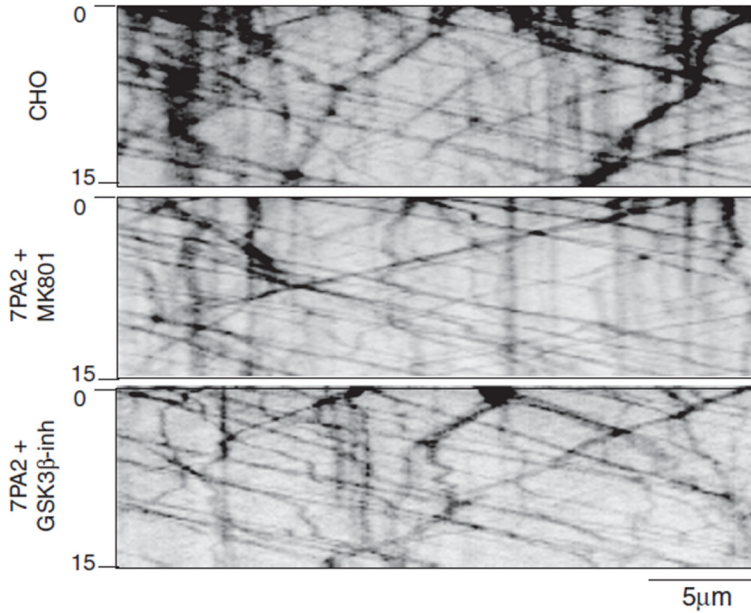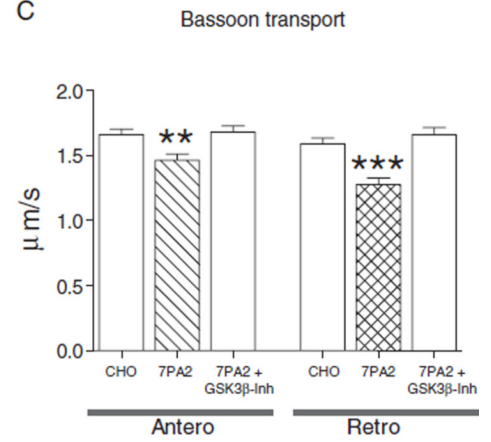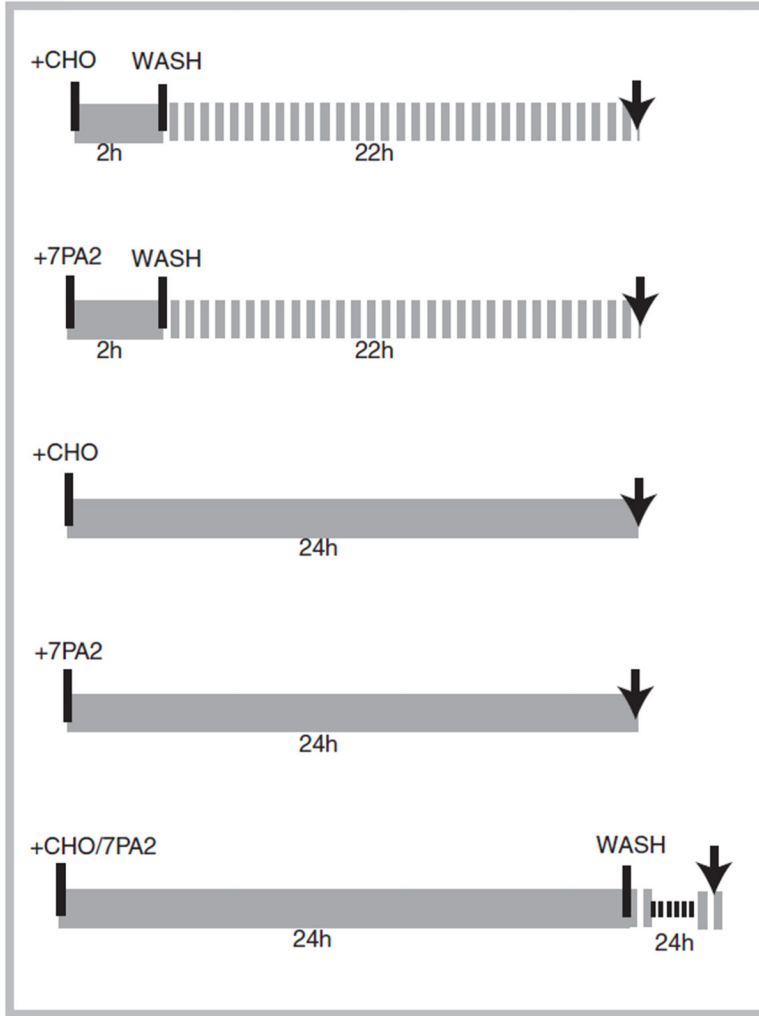
Figure 3. Rescue of Aβ-induced deficits by GSK-3β and NMDA-R inhibitors
Neurons were coincubated with 200 p$_M$ oligomeric-Aβ (7PA2) and the NMDA-R inhibitor
MK-801 (or the selective GSK-3β-inhibitor GSK-VIII) for 2 h, and axonal transport of
synaptophysin and bassoon cargoes was analyzed. A) Representative kymographs from
controls (CHO) and drug-treated axons reflect the similarity of transport kinetics between
the groups. B) All Aβ-induced deficits in axonal transport velocities were completely
rescued by the drug treatments (see Table 1 for numerical data). A caesin kinase (CK)
inhibitor (7) also rescued the transport deficits. $n \approx$ 500–900 moving particles analyzed for
each cargo, from 2 to 4 separate culture sets. *p < 0.05; **p < 0.01; ***p < 0.001; one-way
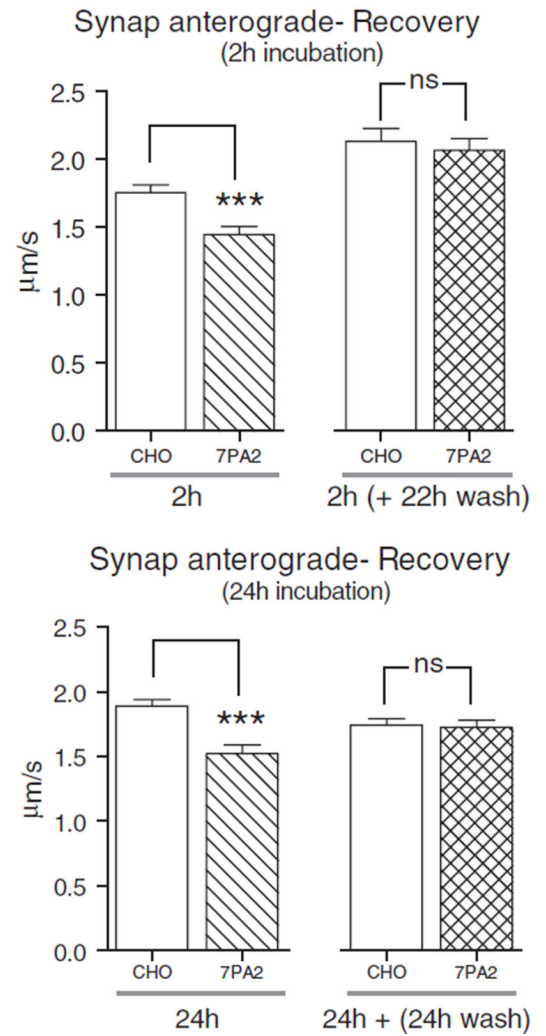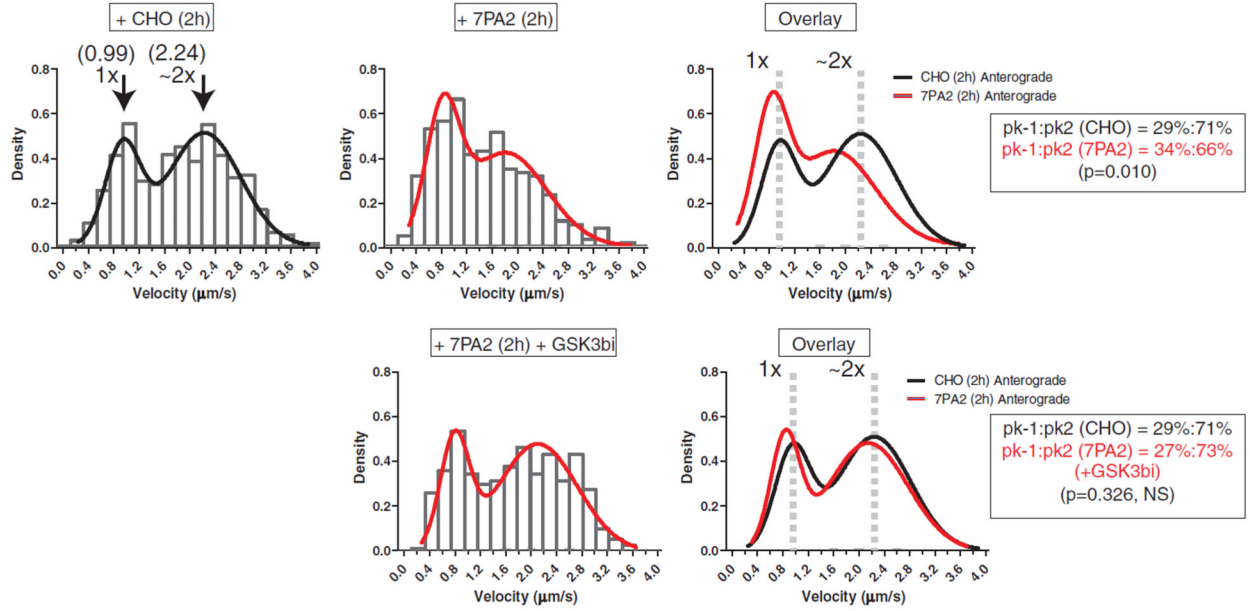ANOVA followed by Dunnet's post hoc test.

Figure 4. Reversibility of Aβ-induced transport deficits upon oligomer washout
A) Design of recovery experiments: Neurons were incubated with 7PA2 (200 p_M Aβ-42) or CHO (0 p_M Aβ-42) for 2/24 h, rinsed extensively and incubated in Aβ-free medium for another 22–24 h (control neurons underwent a mock washout). Arrows represent time-points at which axonal transport of synaptophysin was analyzed. B) Comparison of the average transport velocities of synaptophysin show that washout of oligomers rescued the synaptophysin transport deficits seen at both 2 and 24 h (see Table 1 for numerical data). $n \approx$ 500–600 moving particles analyzed for each cargo, from two separate culture sets. *p < 0.05; **p < 0.01; ***p < 0.001; unpaired *t*-test.
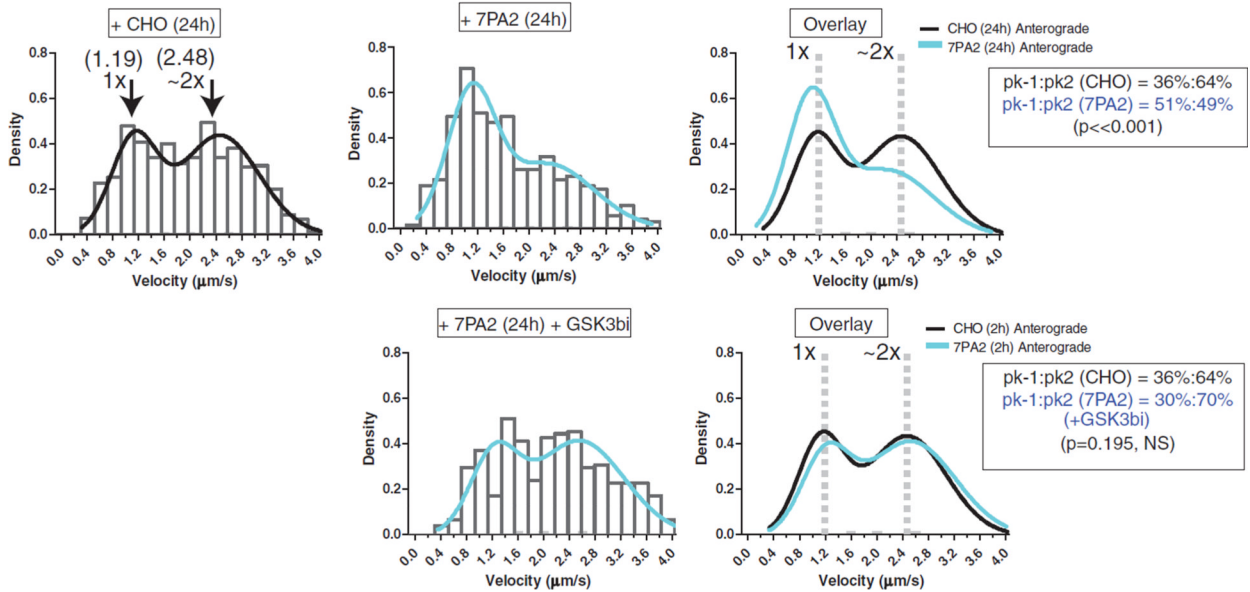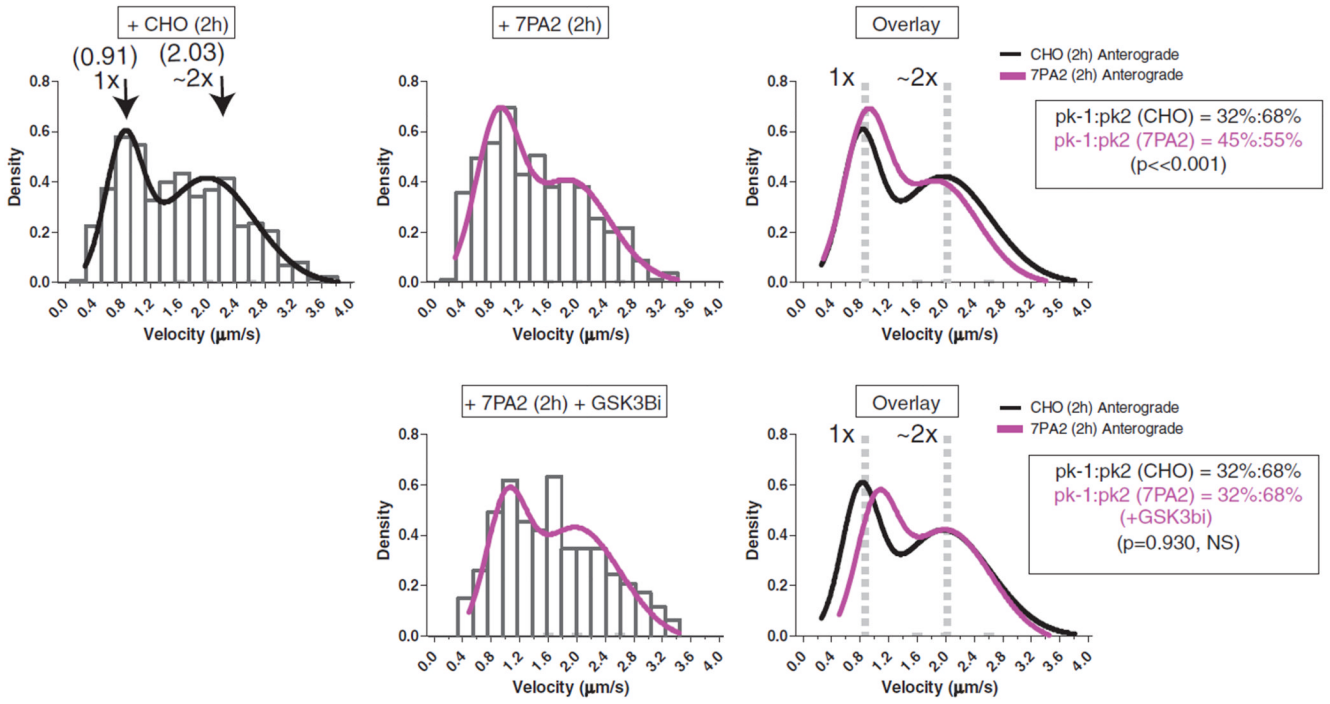
Figure 5. Effects of Aβ-oligomers on axonal transport kinetics
Average velocity histograms of anterograde synaptophysin transport in control axons (CHO, left) or 200 pM oligomeric-Aβ-treated axons (7PA2, middle) with overlaid best fit Gaussian curves obtained from unbiased model-based clustering (see *Materials and Methods*). CHO/7PA2 overlaid curves shown on right. Note that velocity histograms display bimodal peaks with approximate 1× and 2× periodicities that are best fitted by a two-Gaussian function. A) Incubation with 7PA2-media for 2 h resulted in a diminution of the second (2×, faster) peak with expected increases in the relative proportions of the first (1×, slower) peak (top panels, cf. overlaid curves on right). Note that these changes are offset upon GSK3β-inhibition (bottom panels, cf. CHO/7PA2 overlaid Gaussian curves on right). B) Incubation with

7PA2-media for 24 h also resulted in similar attenuation of faster (2×) velocity peaks in the 7PA2 group (cf. CHO/7PA2 curves on top right). As mentioned above, these changes were offset by GSK3β-inhibition (cf. CHO/7PA2 curves on bottom right). Boxes on right show statistics: % areas underlying peak-1/peak-2 (pk1/pk2) and statistical comparison of the relative proportions of the peaks in the CHO/7PA2 groups highlight the 7PA2-mediated alterations of the velocity curves ($p < 0.05$ considered significant, Chi-square test, see *Materials and Methods*).
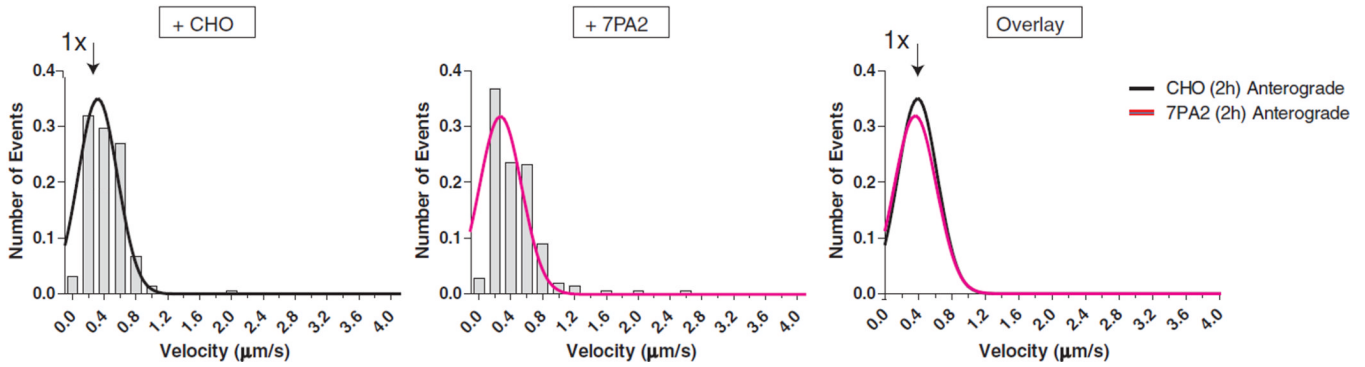
Figure 6. Cluster-mode analysis of bassoon and mitochondrial cargoes

A) Histograms of average velocity distributions of anterogradely moving bassoon cargoes with overlaid Gaussian curves also show a bimodal distribution with approximate 1× and 2× periodicity. Note that there is a significant diminution of the relative proportions of the second (2×, faster) peak upon Aβ incubation (cf. CHO/7PA2 curves on top right). Also, note the offset of these changes upon treatment with GSK-3β inhibitors (lower panels). Boxes on right show statistics: % areas underlying peak-1/peak-2 (pk1/pk2) and statistical comparison of the relative proportions of the peaks in the CHO/7PA2 groups highlight the 7PA2-mediated alterations of the velocity curves (p < 0.05 considered significant, Chi-square test, see *Materials and Methods*). B) Average velocity histograms of mitochondrial transport were best fitted by a single Gaussian, and the CHO/7PA2 Gaussian curves were essentially identical (cf. CHO/7PA2 curves on right).

Figure 7. Biochemical analyses
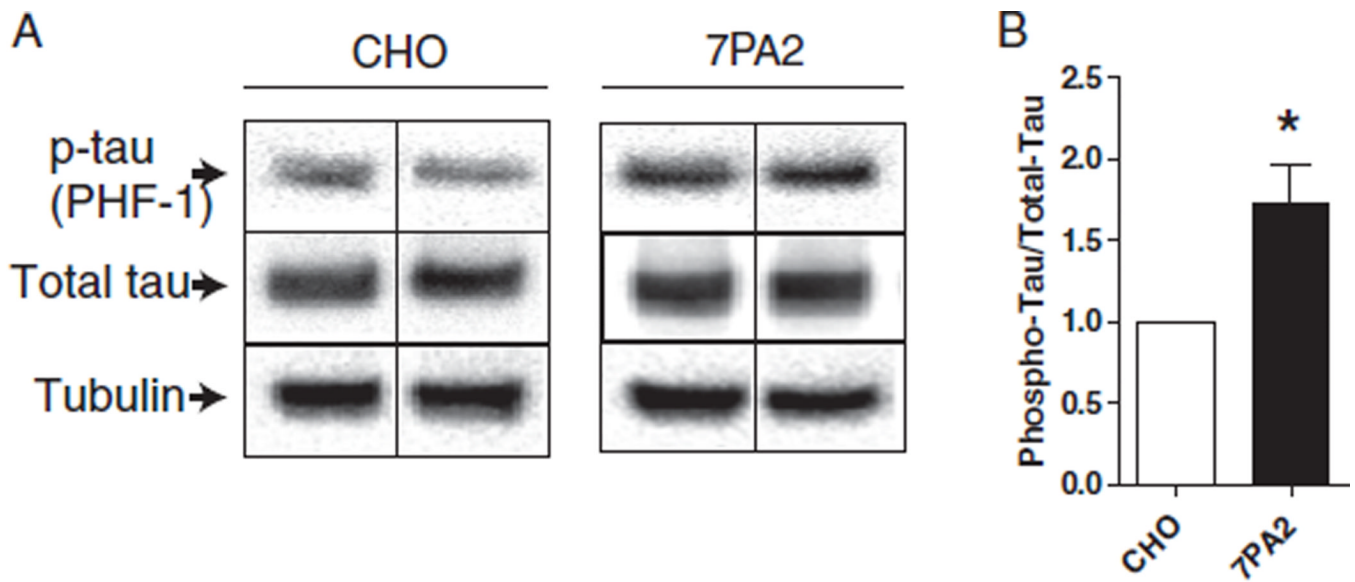Cultured neurons (DIV 14) were incubated with CHO or 7PA2 (1 n$_M$ Aβ-42) media for 24 h, and levels of total tau and phospho-tau were detected by western blotting. Significant increases were seen in phospho-tau levels, as shown in the representative blots (A) and quantification (B). Data represent six separate cultures from three independent experiments ($p < 0.05$, t-test).

Table 1

Average velocities of axonal transport

	Time of incubation	Experiment	Anterograde velocity (μm/second)	Retrograde velocity (μm/second)
Synaptophysin	2 h	CHO	1.81 ± 0.06	1.47 ± 0.06
		7PA2	1.45 ± 0.06 **	1.57 ± 0.11
		7PA2 + GSK-3β	1.75 ± 0.06	1.72 ± 0.09
		7PA2 + MK801	1.95 ± 0.08	1.54 ± 0.07
		7PA2 + D-AP5	1.77 ± 0.06	1.66 ± 0.07
		CHO (+22-h wash)	2.13 ± 0.09	1.60 ± 0.04
		7PA2 (+22-h wash)	2.07 ± 0.09	1.83 ± 0.11
	24 h	CHO	1.89 ± 0.05	1.70 ± 0.05
		7PA2	1.52 ± 0.07 ***	1.74 ± 0.08
		7PA2 + GSK-3β	2.12 ± 0.07 *	1.61 ± 0.06
		CHO (+24-h wash)	1.74 ± 0.05	1.58 ± 0.05
		7PA2 (+24-h wash)	1.73 ± 0.05	1.77 ± 0.09
Bassoon	2 h	CHO	1.66 ± 0.04	1.59 ± 0.04
		7PA2	1.46 ± 0.05 **	1.27 ± 0.05 ***
		7PA2 + GSK-3β	1.68 ± 0.05	1.66 ± 0.05
Mitochondria	2 h	CHO	0.40 ± 0.02	0.41 ± 0.03
		7PA2	0.40 ± 0.03	0.44 ± 0.02

Means reported as averages ± standard error.

* p < 0.05 compared with CHO;

** p < 0.01 compared with CHO;

*** p < 0.001 compared with CHO.

Table 2

Frequencies of axonal transport

	Time of incubation	Experiment	% Anterograde	% Retrograde	% Stationary
Synaptophysin	2 h	CHO	47.55 ± 1.87	24.86 ± 2.03	26.83 ± 2.29
		7PA2	49.85 ± 1.77	22.66 ± 2.34	27.49 ± 2.70
		7PA2 + GSK-3β	50.95 ± 2.83	27.04 ± 2.46	22.71 ± 1.89
		7PA2 + MK801	49.96 ± 1.51	29.49 ± 1.33	20.39 ± 2.05
		7PA2 + D-AP5	49.79 ± 2.80	28.98 ± 2.21	21.23 ± 1.52
		CHO (+22-hwash)	53.40 ± 2.39	24.08 ± 1.97	22.51 ± 1.83
		7PA2 (+22-hwash)	47.63 ± 2.53	26.13 ± 2.78	26.24 ± 2.85
	24 h	CHO	52.63 ± 1.65	24.11 ± 1.64	23.26 ± 1.28
		7PA2	47.37 ± 1.84	28.41 ± 2.27	24.17 ± 2.67
		7PA2 + GSK-3β	50.15 ± 3.24	27.51 ± 2.32	22.34 ± 1.79
		CHO (+24-hwash)	44.91 ± 2.23	21.58 ± 2.16	33.51 ± 3.60
		7PA2 (+24-hwash)	44.81 ± 2.42	28.66 ± 2.37 [*]	26.20 ± 2.02
Bassoon	2 h	CHO	51.97 ± 2.66	21.10 ± 1.81	26.93 ± 2.84
		7PA2	51.43 ± 3.18	22.17 ± 2.13	26.41 ± 3.89
		7PA2 + GSK-3β	44.65 ± 4.00	32.18 ± 3.98 [**]	23.17 ± 3.91
Mitochondria	2 h	CHO	45.37 ± 4.05	20.12 ± 3.02	34.51 ± 5.35
		7PA2	39.23 ± 2.80	22.13 ± 2.46	39.20 ± 4.07

Means reported as averages ± standard error.

[*] $p < 0.05$ compared with CHO;

[**] $p < 0.01$ compared with CHO.